THERMAL CREEP OF ZIRCALOY-4 CLADDING

K. L. MURTY, G. S. CLEVINGER, T. P. PAPAZOGLOU

Nuclear Materials Technology, Babcock & Wilcox Company,
Lynchburg Research Center, P.O. Box 1260, Lynchburg, Virginia 24505, U.S.A.

SUMMARY

Zircaloy-4 is widely used as the cladding material in pressurized water reactors, and a knowledge of creep characteristics of Zircaloy-4 fuel cladding is essential in reliably predicting fuel rod performance. Data on the hoop creep characteristics of Zircaloy tubing were collected at temperatures between 600F and 800F, and at stress levels ranging from 10 ksi to 25 ksi using internal pressurization tests. At low driving forces, exposures as long as 2000 hours were found insufficient to establish steady state creep.

The experimental data at temperatures of 650F to 800F correlate well with an exponential stress dependence, and the activation energy for creep was found to be in excellent agreement with that for self-diffusion. The range of stresses and temperatures is too small to study the overall effect of these variables on the activation energy for creep. The generalized applicable creep equation has the form:

$$\frac{\dot{\varepsilon}_s kT}{DEb} = A \exp\left(B \frac{\sigma}{E}\right), \tag{1}$$

where $\dot{\varepsilon}_s$ = steady-state hoop creep-rate, k = Boltzmann constant, T = test temperature (K), D = self-diffusion coefficient ($= D_0 e^{-QD/RT}$), E = Young's Modulus, b = Burger's vector, σ = applied hoop stress, and A and B are constants. The main advantage of the form of Eq. (1) is that the applied stress and the experimental creep rate are expressed in dimensionless parameters. The experimental steady state creep-rates and those predicted from Eq. (1) agree within a factor of 1.3.

These correlations imply that the mechanism for hoop creep of Zircaloy-4 cladding is characterized by an activation energy of approximately 60 kcal/mole and an activation area of about $20b^2$. In addition, the exponential stress dependence implies that the activation area for creep is stress-independent. These results suggest that the climb of edge dislocations is the rate controlling mechanism for creep of Zircaloy-4.

The transient creep regime was analyzed on the premise that primary creep is directly related to the rate of dispersal of dislocation entanglements by climb. In correlating the primary creep behavior at the temperatures and stress levels used, a plot of creep strain versus $\dot{\varepsilon}_s t$ indicated that data at different temperatures and stresses fall on a universal creep curve. An Avrami-type equation is shown to be a good first approximation in describing the universal curve. The fundamental difference between this formulation and the more familiar Andrade's $t^{1/3}$ law is that the initial creep rate (at $t = 0$) is regarded finite here.

1. Introduction

Zircaloy-4 is widely used as the fuel cladding material in pressurized water reactors and a knowledge of its creep characteristics is essential in predicting fuel rod performance. The objective of the present study is to generate creep data as a function of test temperature and applied internal pressure and to correlate the experimental data with phenomenological theories of creep. Correlations were attempted in the steady-state and primary creep regimes. The use of internal pressurization of tube specimens in the creep tests was predicated on the requirement for representative data on the characteristic response of the material to a given level of temperature and stress. This approach provided a uniform and stable stress distribution, compared with that achieved during external (compressive) pressurization where the complicating effects of tubing ovalization are introduced.

2. Experimental Details

2.1 Experimental System

The system was designed to maintain optimum control of temperature and pressure during the creep exposure. It consisted primarily of a fluidized bed thermocouple calibration bath and a closely monitored gas evacuation and pressurization system. A cluster of six Zircaloy tube specimens was welded to a common pressurized manifold (Figure 1). The specimen assembly was encapsulated in a stainless steel can that could be evacuated and back-filled with helium. The creep can was then immersed in the fluid bed furnace, and the pressure and temperature of the specimens were continuously monitored throughout the exposure.

2.2 Specimen Characterization and Assembly Procedures

Cold-worked stress-relieved Zircaloy-4 cladding was used in this study. Pedigree characterization of the outer diameter of each specimen was achieved with a matched dual-transducer profilometer which generated a helical scan along the length of the tube. The diameters were also remeasured at several stations along each tube with a digital micrometer (accurate to $\pm$ 0.2 mil) after the specimens were welded into their manifold.

Each specimen was internally fitted with a stainless steel mandrel to reduce the gas required for pressurization. The specimens were then welded into the manifold assembly that was connected to a Swagelok union which, in turn, was butt-welded to the lid of a stainless steel outer containment. The entire assembly was then lip-welded to the can and attached to the pressurization system. The container was opened after specified exposure periods by milling the circumferential lip weld and rewelding it following examination of the specimens.

2.3 Temperature and Pressure Control

The creep cans were heated in fluidized bed thermocouple calibration baths controlled to better than $\pm$ 1F. Each fluidized bed furnace could accommodate up to three creep assemblies, but only two were normally used at a time to ensure proper bath fluidization. Excellent temperature uniformity (< 2F) was achieved throughout the usable space in the fluidized bed furnace. Specimen pressure was monitored through in-line pressure gauges accurate to 25 psi. The pressure could be adjusted with greater precision by an

in-line Heise gauge accurate to ± 5 psi. Atmospheric pressure was maintained in the protective cover gas in the cans.

3. Experimental Results

The range of experimental conditions for the creep study included testing at five temperatures and four stress levels. The various combinations of temperature, hoop stress and accumulated creep exposure time for each test condition are shown in Figure 2. At low driving forces (low temperature and /or pressure), exposures of up to ∿ 3000 hours were found insufficient to reach the secondary creep regime. In tests where the accumulated diametral strains were equal to or higher than 1%, the pressure was adjusted to hold the hoop stress constant.

Figure 3 illustrates the effect of stress at a constant temperature. The effect of temperature on creep strain is depicted in Figure 4 at a constant stress. Several general features of the data deserve special mention, particularly the regularity of the strain-time curves with increasing driving force. If primary creep is faster for a given set of test conditions, then steady-state creep also proceeds at a faster rate. The curves do not cross; therefore, comparison of strains at some specified exposure time yields a reasonable estimate of relative creep behavior over the entire range of exposure time. A quantitative description of this feature is given later.

To verify that the interruption of the tests had no significant effect on the data, the test at 750F and 20 ksi was duplicated with a single run to 1200 hours. No differences were detected in the strains between the two types of tests so that the results for the general tests were judged to be unaffected by the interruptions required to perform interim measurements.

4. Creep Data Correlations

4.1 Steady-State Creep

To characterize the temperature and stress dependence of the secondary creep rate of the cladding, a general equation of the form

$$\dot{\varepsilon}_s = A' e^{-\Delta H/RT}, \qquad (1)$$

was first assumed. Here $\dot{\varepsilon}_s$ is the minimum creep rate obtained from the experimental creep curves and ΔH is the activation energy for creep. A' is a function of the applied stress; either a power function ($\propto \sigma^n$) or an exponential function ($e^{\beta\sigma}$) depending on the stress level [1]. The activation energy, ΔH, was evaluated from the experimental data as a function of temperature at a constant hoop stress of 20 ksi. A least squares analysis of that data yielded a value of 64 kcal/mole for the activation energy. This is an apparent activation energy for creep and a true value can be derived by correcting for the temperature variation of the elastic modulus [2]. The datum at 600F was excluded from the above analysis since, as will be clear later, true steady-state conditions were not attained even after 2000 hours' exposure. Hence, the minimum creep rate obtained was still higher than the true steady-state rate. The above value of 64 kcal/mole for the activation energy compares with that for self-diffusion in Zr - 1.3% Sn (62 kcal/mole) determined by Lyashenko [3].

The close agreement of the activation energy for creep as determined above and that for self-diffusion suggests a diffusion controlled creep mechanism. Using Dorn's quasi-theoretical approach [4], the following creep equation is given in terms of dimensionless parameters,

$$\frac{\dot{\varepsilon} kT}{DEb} = f\left(\frac{\sigma}{E}\right), \tag{2}$$

where

$$f\left(\frac{\sigma}{E}\right) = \alpha \left(\frac{\sigma}{E}\right)^n \text{ , for } \sigma \lesssim 10^{-3}E$$

and

$$f\left(\frac{\sigma}{E}\right) = \beta\, e^{B(\sigma/E)} \text{ for } \sigma \gtrsim 10^{-3}E.$$

In eq. (2)

$\dot{\varepsilon}$ = steady-state creep rate

σ = applied stress

E = elastic modulus

α, β = constants

T = test temperature (°K)

$D = D_o e^{-Q/RT}$ = diffusion coefficient

b = Burger's vector

k = Boltzmann constant.

To determine the modulus-compensated activation energy for creep, the experimental data are plotted in Figure 5 as $\ln\left(\frac{\dot{\varepsilon} T}{E}\right)$ versus $1/T$ at a constant value for σ/E of 2.0×10^{-3}. A value of 59.5 kcal/mole was derived for the true activation energy for creep from Figure 5. This is in excellent agreement with the literature data [5] for high temperature creep of pure zirconium and zirconium alloys. Within experimental scatter, this value may be regarded as equal to that for self-diffusion for all practical purposes.

It is noted that all the present experimental data are such that

$$\sigma > 10^{-3}E \text{ and } \dot{\varepsilon} > 10^{9}D, \tag{3}$$

where $D = 5 \exp(-62{,}000/RT)\ \text{cm}^2/\text{sec}$ [3].

From eq. (2) and Sherby's rule of thumb [1], we note that the exponential stress dependence of the creep rate is applicable to the present data. Figure 6 is a semi-log plot of $\dot{\varepsilon} kT/DEb$ versus σ/E. The following creep equation is then obtained with a correlation factor of 0.994 to the experimental results:

$$\frac{\dot{\varepsilon} kT}{DEb} = A\, e^{B(\sigma/E)}, \tag{4}$$

where A and B are constants. Again, the data at 600F were not included for reasons stated earlier. Table I lists the test temperature, applied hoop stress, and the ratio of experimental to calculated strain rate. The agreement is good, with the experimental value differing by a factor of 1.3 in the worst case. The fact that this ratio is quite large for 600F data indicates that the experimental data at 600F fell in the primary creep region and true steady-states were not attained.

The validity of the correlation established by eq. (4) implies that the rate controlling mechanism for creep deformation under the conditions used in this program can be characterized by a stress-independent activation area A*, defined as

$$A^* = \frac{2kT}{b} \left(\frac{\partial \ln \dot{\varepsilon}}{\partial \sigma}\right)_T. \tag{5}$$

Physically, the activation area may be interpreted as the area swept out by a dislocation segment in moving over a barrier on its slip plane. The magnitude of the activation area depends on the strength and nature of the obstacles and the rate controlling step. The range of values of A* extracted from the present program data ($17b^2$ - $23b^2$) can be compared with the theoretical values predicted for various types of dislocation mechanisms known to control creep [6].

Having an activation energy for creep of approximately 60 kcal/mole suggests a diffusion-controlled creep mechanism, such as climb of the edge dislocations and nonconservative motion of jogged screw dislocations. The activation area values of $\sim 20b^2$ suggest that the climb of the edge dislocations is the rate controlling step.

4.2 Transient Creep

In the following treatment we utilize the analyses and procedures adopted by Dorn and his coworkers [7] to explain the primary creep behavior of various metals. They showed that under temperatures and stresses at which metals exhibit climb-controlled creep, primary creep can be directly related to the rate of dispersal of dislocation entanglements by climb. Assuming that this dispersal follows unimolecular reaction kinetics, we can write

$$\frac{d(\dot{\varepsilon} - \dot{\varepsilon}_s)}{dt} = -\beta \dot{\varepsilon}_s (\dot{\varepsilon} - \dot{\varepsilon}_s), \tag{6}$$

where $\dot{\varepsilon}$ is the creep rate at time t, $\dot{\varepsilon}_s$ is the steady-state creep-rate and $\beta\dot{\varepsilon}_s$ the rate constant. Thus,

$$\varepsilon - \varepsilon_o = \dot{\varepsilon}_s t + \frac{\dot{\varepsilon}_i - \dot{\varepsilon}_s}{\beta \dot{\varepsilon}_s} \left\{1 - e^{-\beta \dot{\varepsilon}_s t}\right\}, \tag{7}$$

where ε_o is the strain and $\dot{\varepsilon}_i$ is the initial creep rate at t = 0. Therefore,

$$\varepsilon - \varepsilon_o = \dot{\varepsilon}_s t + \varepsilon_T \left(1 - e^{-\beta \dot{\varepsilon}_s t}\right), \tag{8}$$

with the transient creep strain, $\varepsilon_T = (\dot{\varepsilon}_i - \dot{\varepsilon}_s)/\beta\dot{\varepsilon}_s$. It is important to realize that the kinetics of reaction are the same in both primary and steady-state stages, a fact established for many metals [7]. It then follows that

$$\dot{\varepsilon}_i = \kappa\, \dot{\varepsilon}_s, \tag{9}$$

where κ is greater than unity since we are concerned here with normal or decelerating primary creep. From extensive correlations on creep characteristics in various metals, Dorn [7] observed that the constants κ, β and ε_T are independent of temperature and stress but are characteristic of the material in question. The fundamental difference between this formulation and the familiar Andrade's $t^{1/3}$-law is that $\dot{\varepsilon}_i$ is regarded finite here, whereas Andrade's equation predicts infinite initial creep rates.

Eqs. (7) and (8) imply the existence of a universal transient and steady-state creep curve given by

$$\varepsilon - \varepsilon_o = f(\dot{\varepsilon}_s t) = F\left\{\frac{DEb}{kT}\; e^{B\sigma/E} t\right\}, \tag{10}$$

where the function F is derived from eq. (4) and is applicable to steady-state creep in the material used in this investigation.

For calculations in the present data, ε_o may be regarded as negligible. This may not hold at high driving forces, however, and will lead to more scatter in the correlation. Figure 7 is a plot of creep strain versus $\left(A \frac{DEb}{kT} e^{B\sigma/E}\right)t$ for the various stress and temperature levels employed here. Excepting the data at very low driving forces (600F tests), the rest of the data follow a single curve within expected scatter. The majority of the data follow a single curve within expected scatter. The majority of the scatter stems from neglecting ε_o and not properly accounting for variations in the initial loading procedure. The 600F data are shown with circled points to indicate that the values for $\dot{\varepsilon}_s$ used to derive these data are not representative of the true steady states. Indeed, a back extrapolation, assuming that the 600F data should also follow the universal curve in Figure 7, yields steady-state rates comparable to those evaluated from eq. (4) as shown below

$$\left.\begin{aligned} &\dot{\varepsilon}_s \text{ (universal curve)} = 0.81\ \dot{\varepsilon}_s \text{ (eq. 4)}, \quad 20 \text{ ksi} \\ &\dot{\varepsilon}_s \text{ (universal curve)} = 1.36\ \dot{\varepsilon}_s \text{ (eq. 4)}, \quad 25 \text{ ksi} \end{aligned}\right\} \text{ 600F.} \tag{11}$$

Such an agreement attests to the validity of the present formulation based on eq. (10).

Unfortunately, it is difficult to determine $\dot{\varepsilon}_i$ and ε_T from the present data. The parameters ε_T and β in eq. (10) were determined from the average curve through the experimental data in Figure 7 as follows: A value for ε_T was obtained by extrapolating the linear portion of the curve at large values of weighted-time back to zero and noting the strain intercept. The rate constant β was determined at one half of the transient strain ε_T where

$$\beta = \left. \frac{\ell n 2}{\left(A \frac{DEb}{kT} e^{B\sigma/E} \right) t} \right|_{\varepsilon = \varepsilon_{T/2}} \tag{12}$$

The best values for ε_T and β were found to be 0.005 and 1500, respectively. Since

$$\varepsilon_T = \frac{\dot{\varepsilon}_i - \dot{\varepsilon}_s}{\beta \dot{\varepsilon}_s} = \frac{\kappa - 1}{\beta}, \tag{13}$$

$$\kappa = \frac{\dot{\varepsilon}_i}{\dot{\varepsilon}_s} = 1 + \varepsilon_T \beta \quad . \tag{14}$$

A value of 8.5 was derived for κ in the present work. This value is in good agreement with those derived for various fcc and bcc metals [7]. The creep curves predicted by the above model and experimental data are shown in Figure 8 for various stress levels at 700F. The model results are in good agreement with the experimental data at high driving forces. The predicted strains at low driving forces are somewhat lower than the experimental values, especially at short exposures and low strain values. This disparity results from insufficient data to properly evaluate the rate constants applicable to the correlation.

From a comparison of the experimental data with the universal curve, the transition from primary to secondary creep was noted at a strain, ε_{tr}, of approximately 0.75%. The strain-rate during the transient stage may be described by

$$\dot{\varepsilon} = \dot{\varepsilon}_s \left(1 + \varepsilon_T \beta \, e^{-\beta \dot{\varepsilon}_s t}\right), \tag{15}$$

so that, using eq. (4), we can write the general form

$$\dot{\varepsilon} = C_1 e^{C_2 \sigma} \left(1 + \varepsilon_T \beta \, e^{-A\beta e^{C_2 \sigma} t}\right), \tag{16}$$

where C_1 and C_2 are temperature dependent. Staehle's work at Kraftwerk Union (KWU) [8] indicated that, irrespective of the test temperature and stress, steady-state creep was observed for strains above $\sim$ 0.8% and transient creep for lower hoop strains. In addition, a computer fit to his data in primary creep yielded [8]

$$\dot{\varepsilon} = \beta_1 \, e^{\beta_2 (e^{-\mu})t} \quad \text{for } \varepsilon < 0.8\%.$$

The correlations developed from data collected in the present program are in accord with these observations.

5. Summary and Conclusions

Data on the creep characteristics of Zircaloy-4 cladding were collected at temperatures from 600 to 800F at hoop stress levels ranging from 10 to 25 ksi. At low driving forces, exposures of up to 2000 hours were found insufficient to establish steady-state creep, and the data obtained at 600F were shown to fall within the primary creep regime. The experimental data at temperatures of 650 to 800F correlate well with an exponential stress dependence, and the activation energy for creep was found to be in excellent agreement with that for self-diffusion. The range of experimental stresses and temperatures

did not permit study of the overall effect of these variables on the activation energy for creep. The generalized applicable creep equation has the form

$$\frac{\dot{\varepsilon} kT}{DEb} = A \exp\left(B \frac{\sigma}{E}\right) \quad . \tag{17}$$

The experimental creep rates and those predicted from eq. (17) agreed within a factor of 1.3.

These correlations imply that the mechanism for creep in Zircaloy 4 is characterized by an activation energy of approximately 60 kcal/mole and an activation area of about $20b^2$. In addition, the exponential stress dependence implies that the activation area is stress-independent. These results point to the climb of edge dislocations as the rate controlling mechanism.

In correlating the transient behavior at the temperatures and stress levels used in this program, the following functional dependence for creep was determined:

$$\varepsilon = f\ (\dot{\varepsilon}_s t) = F\ \left(\frac{ADEb}{kT}\ e^{B\sigma/E} t\right). \tag{18}$$

A plot of ε versus $\dot{\varepsilon}_s t$ indicated that data at different stresses and temperatures fall on a universal creep curve. Values for steady-state creep rates at 600F - 20 ksi and 600F - 25 ksi conditions, derived from the universal curve, agreed with the predictions based on correlations of steady-state data. This is indicative of the general validity of the present transient creep correlations.

Assuming that the kinetics of reaction are the same in both the primary and steady-state creep regimes, creep strain as a function of time may be given by

$$\varepsilon = \varepsilon_o + \dot{\varepsilon}_s t + \varepsilon_T\ (1 - e^{-\beta \dot{\varepsilon}_s t}). \tag{19}$$

This equation, where $\varepsilon_o = 0$, $\varepsilon_T = 0.005$ and $\beta = 1500$, predicts the experimental creep data satisfactorily. These results imply that the initial creep rate,

$$\dot{\varepsilon}_1 = 8.5\ \dot{\varepsilon}_s. \tag{20}$$

It was found that regardless of the level of driving force, at strains below about 0.0075, the creep rate diminishes with time (primary creep), while at higher strains the creep rate is independent of time (steady state).

Acknowledgments

Acknowledgments are due to Mr. F. R. Foster for skillfully carrying out the experiments and to Mrs. Phine Shaeff for typing the manuscript. This work was sponsored by the Nuclear Power Generation Division of the Babcock and Wilcox Company.

Table I. Comparison of Experimental and Calculated Secondary Creep Rates

Temp, F	σ, ksi	$\dot{\varepsilon}_{exp.}/\dot{\varepsilon}_{pred.}$
800	10	0.88
	20	1.07
750	10	1.08
	15	1.16
	20	0.85
700	10	1.30
	15	0.88
	20	1.18
	25	0.95
650	15	1.10
	20	1.12
	25	1.32
600	20	6.00(*)
	25	2.95(*)

(*) Steady states not attained.

References

[1] Sherby, O. D., and Burke, P. M., "Mechanical Behavior of Crystalline Solids at Elevated Temperature," Prog. Mat. Sci., 13, 325 (1967).

[2] Murty, K. L., Gold, M., and Ruoff, A. L., "High-Temperature Creep Mechanisms in α-Iron and other Metals," J. Appl. Phys., 41, 4917 (1970).

[3] Lyashenko, V. S., Bykor, V. N., and Pavlinov, L. V., "A Study of Self-Diffusion in Zirconium and its Alloys with Tin," Fiz. Metalle Metalloved, 8, 362 (1959); Phys. Metals Metallograph, 8, 40 (1960).

[4] Bird, J. E., Mukherjee, A. K., and Dorn, J. E., in "Quantitative Relation Between Properties and Microstructure," Israel University Press (1969), pp. 255 - 342.

[5] Douglas, D. L., Atomic Energy Review, 1964, and The Metallurgy of Zirconium (Supplement 1971), IAEA, Vienna.

[6] Conrad, H., "Thermally Activated Deformation in Metals," J. Metals, 16, 582 (1964).

[7] Amin, K. E., Mukherjee, A. K., and Dorn, J. E., "A Universal Law for High-Temperature Diffusion Controlled Transient Creep," J. Mech. Phys. Solids, 18, 413 (1970).

[8] Staehle, H., "KWU Cladding Creep Characterization," ASTM Conference B10-02, Boston, May (1974).

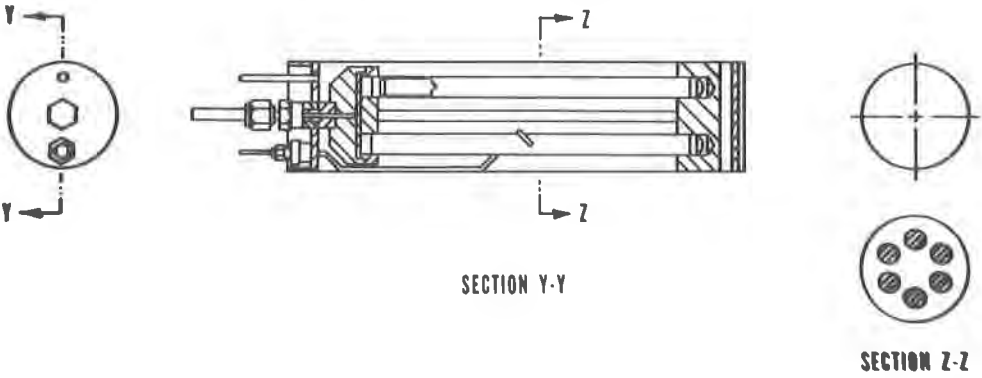

Figure 1. Zircaloy Tube Specimens Welded to Common Pressurization Manifold

T, F / σ, ksi	600	650	700	750	800
10			500	300	250
15		2000	800	300	
20	2065	3020	800	1200	
25	2062	580	500		

Figure 2. Scope of Experimental Conditions for Creep Testing. Numbers Indicate Total Exposure Periods (hours).

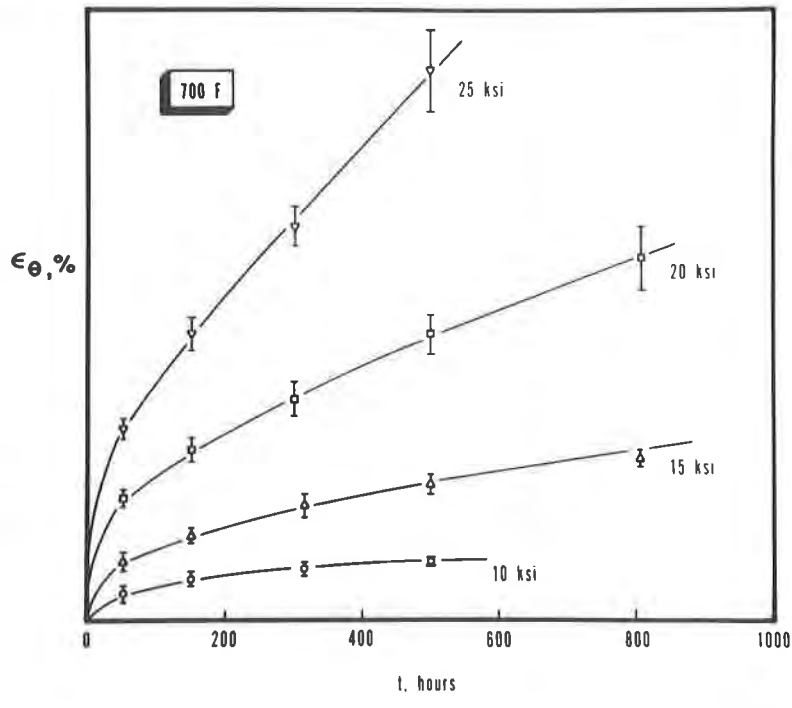

Figure 3. Effect of Stress on Creep Curves at 700F

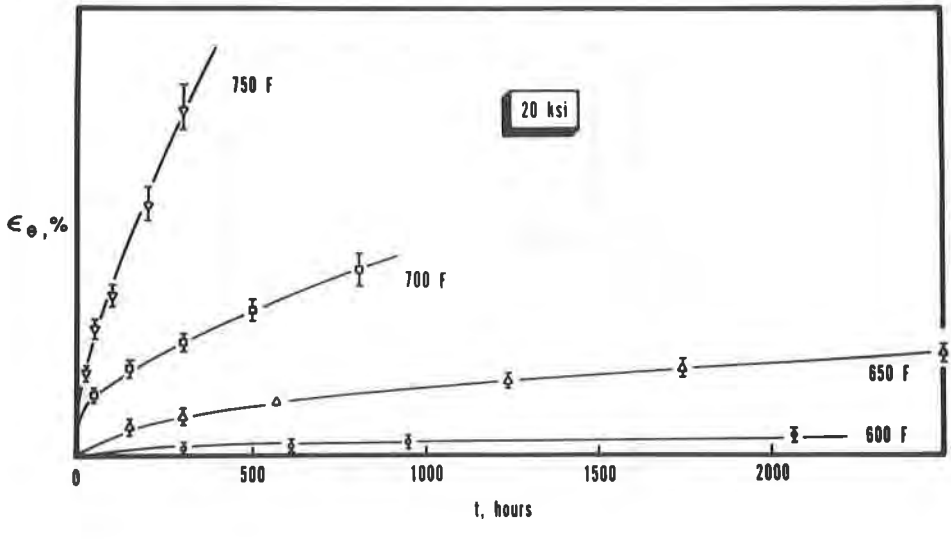

Figure 4. Effect of Temperature on Creep Curves at 20 ksi

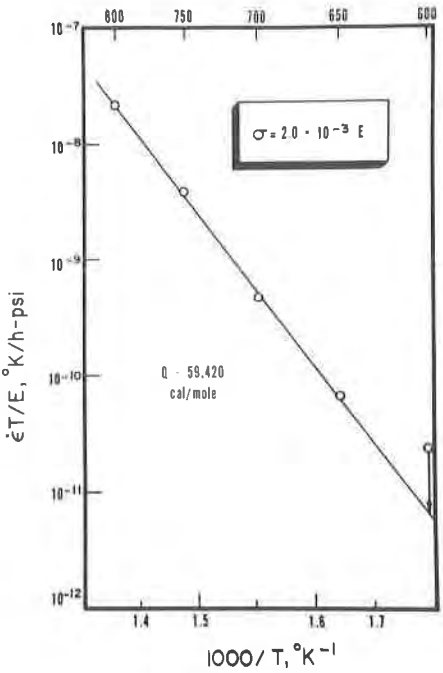

Figure 5. Arrhenius Plot of Modulus-Compensated Strain-Rate Plotted as $\ell n(\dot{\epsilon}T/E)$ versus 1/T at Constant σ/E

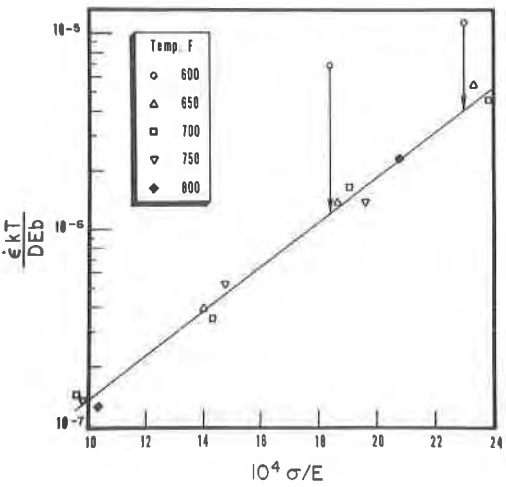

Figure 6. Stress Dependency of Creep Rate Plotted in Dimensionless Parameters as ℓn ($\dot{\epsilon}$kT/DEb) versus (σ/E)

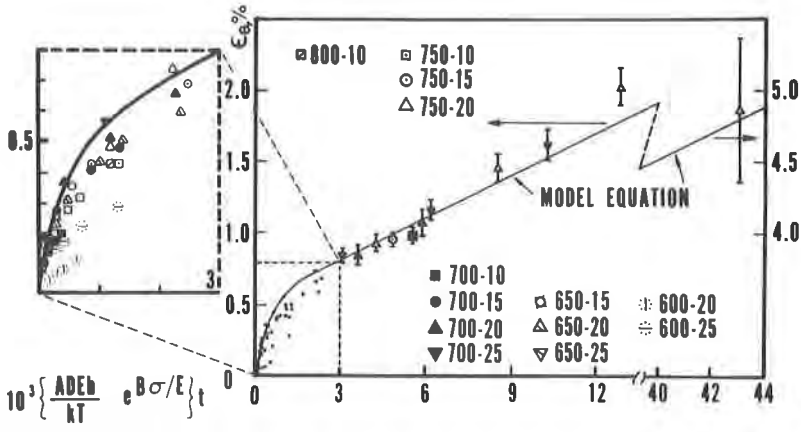

Figure 7. Creep Strain (ε) Versus Weighted Time Illustrating Universal Behavior and Comparison with Theory

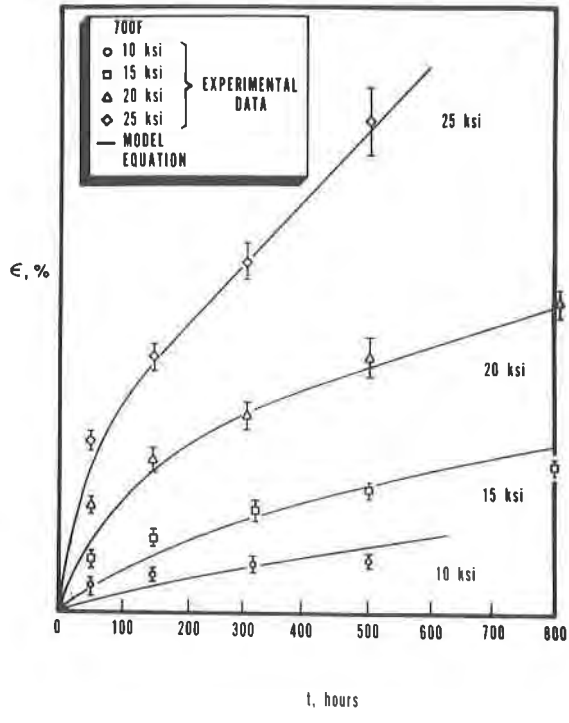

Figure 8. Comparison of Experimental Data and Theoretical Curves at 700F